ChemComm

COMMUNICATION

View Article Online
View Journal | View Issue

Cite this: *Chem. Commun.*, 2017, 53, 3994

Received 20th January 2017,
Accepted 17th March 2017

DOI: 10.1039/c7cc00554g

rsc.li/chemcomm

Encapsulation induced aggregation: a self-assembly strategy for weakly pi-stacking chromophores†

Soumik Sao, Ishita Mukherjee, Priyadarsi De and Debangshu Chaudhuri*

Molecular assembly of weakly pi-stacking core-substituted naphthalene diimides (cNDIs) requires the participation of strong side-group interactions. Spatial confinement within a micellar core leads to locally elevated concentrations and reduced entropy that drives a rapid aggregation, often followed by a slower aggregate reorganization. Fast aggregation kinetics leads to self-sorting of aggregates.

Self-assembly of molecular chromophores is a powerful and versatile strategy for designing functional nanostructures that exhibit fascinating electronic and optical properties, distinct from their molecular constituents.[1,2] At the heart of self-assembly lies weak non-covalent interactions,[3] which to a large extent dictate the packing and relative orientation of the chromophores,[4] and thus determine the nature and the strength of electronic interaction between them. Pi-stacking is one such non-covalent interaction that has been widely employed in a host of self-assembled architectures. Being an interaction between molecular quadrupole moments,[5] pi-stacking is inherently weak. Only in a handful of cases involving extended pi-systems with large positive quadrupole moments,[6] is pi-stacking appreciably strong to guide a self-assembly.

Naphthalene diimides (NDIs) are a class of electron-deficient molecules that readily form pi-stacked aggregates with exceptional n-type semiconducting properties.[7] In contrast, core-substituted NDIs (cNDIs) with electron-donating groups are far less amenable to pi-stacking, owing to a drastically reduced quadrupolar moment.[8] Consequently, self-assembly of these chromophores usually requires a stronger side-group participation through solvophobic interactions or H-bonding,[9] in turn necessitating the need for appropriate functionalization of the parent chromophore. In the search for a general aggregation strategy for weakly pi-stacking chromophores, we shifted our focus from the molecule to its environment. While the importance of non-covalent interactions between chromophore and solvent molecules cannot be overstated,[10] the role of physical confinement in dye aggregation has not been adequately explored.[11] In this work, we demonstrate aggregation of weakly pi-stacking cNDIs within the hydrophobic core of a polymer micelle. Though the enthalpic gain associated with cNDI pi-stacking is poor, its physical confinement within the micellar core offers a two-fold advantage: there is a significant increase in the local concentration of the dye, along with a marked reduction in the total entropy such that even a small enthalpic gain can lead to spontaneous aggregation.

Fig. 1a presents the molecular structures of the three model dye compounds under investigation. R-cNDI and 2R-cNDI are core-substituted NDIs with one and two amino groups,[12]

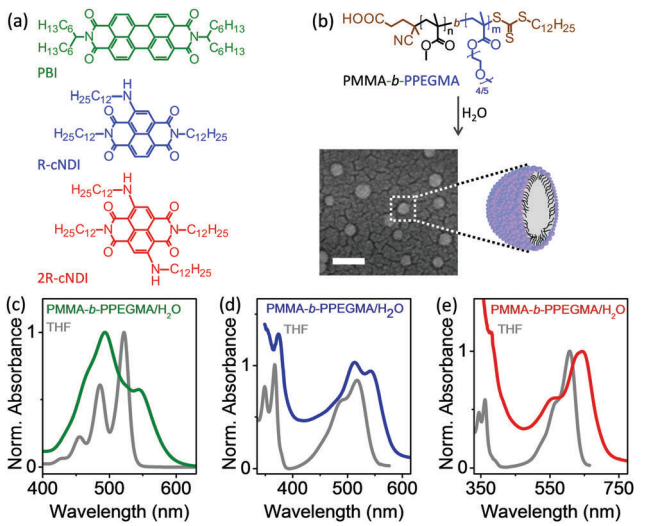

Fig. 1 Encapsulation induced aggregation. (a) Molecular structures of the dyes: symmetric perylene bisimide (PBI), core-substituted NDI with one and two amino substituents, R-cNDI and 2R-cNDI, (b) amphiphilic copolymer PMMA-*b*-PPEGMA. FE-SEM micrograph of polymer micelles (scale bar 100 nm). Optical absorption spectra of aggregated, (c) PBI (green), (d) R-cNDI (blue) and (e) 2R-cNDI (red) in the aqueous suspension of PMMA-*b*-PPEGMA micelles. Spectra of the corresponding monomolecular dyes in THF are shown (grey lines) for comparison.

Department of Chemical Sciences and Centre for Advanced Functional Materials (CAFM), Indian Institute of Science Education and Research (IISER) Kolkata, Mohanpur 741246, India. E-mail: dchaudhuri@iiserkol.ac.in

† Electronic supplementary information (ESI) available: Synthesis and characterization of dyes and the copolymer; control experiments and details of spectral decomposition. See DOI: 10.1039/c7cc00554g

respectively. Additionally, we included a symmetric perylene bisimide (PBI) as a reference compound, whose aggregation behaviour in solution is well documented.[6] All three dye molecules were designed to bear hydrocarbon side chains such that the dominant non-covalent interaction driving molecular aggregation was pi-stacking.‡ The polymer, PMMA-*b*-PPEGMA consists of a hydrophobic poly(methyl methacrylate) (PMMA) block and a hydrophilic poly(poly(ethylene glycol) methyl ether methacrylate) (PPEGMA) block. Owing to its amphiphilicity, PMMA-*b*-PPEGMA spontaneously assembles in water into spherical micelles (~35 nm diameter) (see Fig. 1b), wherein the PMMA block forms the hydrophobic core of the micelle and the PEGMA block forms the outer shell. Compared to low-molecular weight surfactant micelles, polymeric micelles are more stable, undergoing a slower rate of dissociation,[13] thus ensuring retention of dye molecules for a longer period of time. Dye encapsulation within the micelle was carried out by mixing a solution of the dye in non-aggregating (Fig. S8, ESI†) tetrahydrofuran (THF) with an aqueous suspension of pre-formed polymer micelles in 1 : 37 v/v ratio (see the ESI†). In the absence of polymer micelles, excess water causes a rapid and complete precipitation of the hydrophobic dye, as confirmed in a control experiment (Fig. S9, ESI†). However when co-dispersed with polymer micelles, a significant fraction of the dye remains in the solution phase, imparting a distinct colour (Fig. S10, ESI†).

Fig. 1c–e present the optical absorption spectra of the dyes in THF *vis-à-vis* in an aqueous suspension of polymer micelles. We first take the case of the reference PBI (Fig. 1c); its absorption spectrum in THF is characterized by three vibronic peaks at 521 (0–0), 486 (0–1) and 455 nm (0–2), typical of a monomolecular PBI species.[6] Dispersing in an aqueous suspension of polymer micelles causes a distinct reversal in the relative absorbance of 0–0 and 0–1 vibronic features (A_{0-0} and A_{0-1}), indicating a cofacial (H-type) aggregation of PBI molecules. The appearance of a new absorption peak at 544 nm suggests that PBI molecules are rotationally displaced with respect to each other in the aggregate.[14] An independent validation of H-type aggregation is also obtained from the fact that the characteristic photoluminescence (PL) of molecular PBI is replaced by a weaker, broader and red-shifted excimer PL (Fig. S11, ESI†).[6,15] Clearly PBI, which has a strong propensity for pi-stacking, undergoes spontaneous aggregation in the presence of polymeric micelles. Prompted by this, we turned our attention to the weakly pi-stacking cNDI dyes. R-cNDI exhibits a very similar behaviour to that of the reference PBI. A comparison of its optical absorption spectrum in two different media (Fig. 1d) shows a reversal in the relative absorbance of 0–0 and 0–1 vibronic features of the S_0–S_1 band.[16] This along with the fact that the PL of R-cNDI is completely quenched in the presence of polymer micelles (Fig. S12a, ESI†), is consistent with an H-type aggregation. To elucidate the role of the molecular interaction of R-cNDI with the polymer *vis-à-vis* its physical encapsulation within the micelle, a series of control experiments were carried out (see Fig. S13–S15, ESI†) in which interactions of R-cNDI (and 2R-cNDI) with hydrophilic PEGMA, hydrophobic PMMA and un-micellized PMMA-*b*-PPEGMA were studied. Our results show that molecular interactions between the cNDI dyes and the copolymer can neither stabilize the dye against precipitation in aqueous medium, nor can it promote any aggregation. Thus, the only way the dye could remain dispersed in the aqueous phase is by means of encapsulation within the hydrophobic core of the micelle (Fig. S16, ESI†). Once encapsulated, the local concentration of dye inside the micellar core is high enough to assist pi-stacking/aggregation. Encapsulation of di-substituted 2R-cNDI within the polymer micelle gives rise to a significantly complex absorption spectrum (Fig. 1e) that cannot be rationalized in terms of a change in the relative absorbance of the vibronic features. Subsequent time dependent absorption spectroscopy indicates the presence of multiple aggregate species and complex aggregation pathways within the micelle. These observations are particularly remarkable in light of the fact that both R-cNDI and 2R-cNDI remain non-aggregated in strongly aggregating solvents such as methylcyclohexane, even at high concentrations (see Fig. S8b and d, ESI†).

The steady state results presented so far demonstrate aggregation of weakly pi-stacking cNDIs by means of confinement inside polymer micelles. However, two aspects associated with the process warrant further investigation. The first one concerns the kinetics of encapsulation. It is evident that in a predominantly aqueous environment, dye encapsulation must compete with precipitation, a phenomenon that is both rapid as well as quantitative (Fig. S9, ESI†). The other issue pertains to the local environment within the micellar core and its effect on the exact nature of dye aggregation. The second point is particularly relevant in the case of 2R-cNDI that shows a surprisingly complex steady-state absorption spectrum. In order to gain a better insight into the dynamics of dye encapsulation and its subsequent aggregation we studied the temporal evolution of the absorption spectra of R-cNDI and 2R-cNDI. A solution of dye in THF was injected into an aqueous suspension of PMMA-*b*-PPEGMA micelles (1 : 37 ratio), and immediately filtered through a 450 nm pore-size filter to remove any precipitated dye. The optical absorption spectrum of the filtered solution was measured at different time intervals to monitor the fate of the encapsulated dye. Fig. 2a presents the time-dependent absorption spectrum of R-cNDI. The $t_{initial}$ spectrum, one that is measured within 1 minute of dispersing the dye in the micellar suspension, presents the most striking results. Even in the initial stages of encapsulation, the extent of H-aggregation is nearly complete, as is evident from the A_{0-0}/A_{0-1} ratio. Over the course of next several hours, the absorption spectrum shows no significant change. It is indeed surprising that despite a low volume fraction of polymer micelles, a significant fraction of R-cNDI is so rapidly encapsulated within the micelle. Further, the fact that encapsulation of R-cNDI and its subsequent aggregation cannot be discerned separately, even at a lower concentration (Fig. S17a and c, ESI†) and temperature (Fig. S18a and b, ESI†), highlights the fact that the environment inside the micellar core is strongly favourable for aggregation.

In contrast to R-cNDI, the encapsulation of 2R-cNDI exhibits an interesting dynamics (Fig. 2b). The $t_{initial}$ spectrum of 2R-cNDI is significantly different from and simpler than the corresponding steady state absorption spectrum. A quick comparison with the

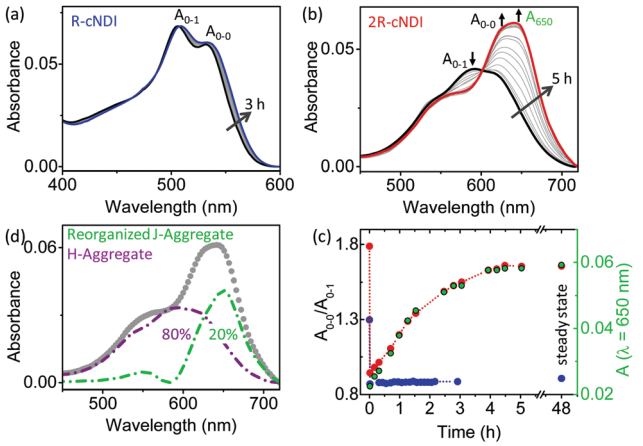

Fig. 2 Temporal evolution of encapsulated dyes at 25 °C. (a) R-cNDI forms H-aggregates instantaneously (black line) and shows little change thereafter (blue line). (b) Reorganization of the initially formed H-aggregated 2R-cNDI (black line) is marked by a gradual increase in the A_{0-0}/A_{0-1} ratio and the rise of a new absorption band at 650 nm (A_{650}) over 5 h duration (red line). (c) Change in the A_{0-0}/A_{0-1} ratio of R-cNDI (blue circle) and 2R-cNDI (red circle) shows the aggregation dynamics of encapsulated dyes. In the case of 2R-cNDI, the increase in A_{650} (green circles) and the A_{0-0}/A_{0-1} ratio follow identical kinetics. A_{650} and A_{0-0}/A_{0-1} values at 48 h correspond to the steady-state spectrum. (d) Spectral decomposition of the 2R-cNDI steady-state spectrum (grey circle) reveals H-(purple) and J-(green) aggregated species in a 1 : 4 ratio.

spectrum of the un-aggregated dye in THF (Fig. S19, ESI†) reveals once again the characteristic signature of H-type aggregation: the A_{0-0}/A_{0-1} ratio decreases from the molecular value of 1.79 to 0.94. Quite expectedly, H-type aggregation is also associated with a complete loss of PL (Fig. S12b, ESI†). Once again, a rapid encapsulation and subsequent aggregation of 2R-cNDI is achieved within the first minute of the experiment. However unlike R-cNDI, the initially formed H-aggregate of 2R-cNDI undergoes a gradual transformation over the next several hours. A cursory examination of the time-series reveals several interesting features: a distinct isosbestic point at 601 nm and a quasi-isosbestic region between 450 and 550 nm. The former indicates a one-to-one reorganization of the initial H-aggregate into a different, but well-defined aggregate species. A quantitative measure of this aggregate reorganization can be obtained from the A_{0-0}/A_{0-1} ratio, which increases from 0.94 to 1.65 over a period of 5 hours. In addition to this, a new absorption feature appears at 650 nm that progressively grows to become the new absorption maxima at longer time scales. Quite remarkably, an increase in the A_{0-0}/A_{0-1} ratio as well as the growth of 650 nm feature (A_{650}) follow an identical kinetics (Fig. 2c), thus suggesting a common underlying cause, associated with the emergence of the reorganized aggregate. This allows us to decompose the absorption spectra of encapsulated 2R-cNDI, $S_{exp}(t)$, as a time-dependent linear combination of only two participating species (see the ESI† for details): the initially formed H-aggregate, $S_H = S_{exp}(t_{initial})$, and the reorganized aggregate, S_R (Fig. 2d and Fig. S17, ESI†).

$$S_{exp}(t) = a_H(t)S_{exp}(t_{initial}) + (1 - a_H)S_R$$

The spectrum of the reorganized aggregate can therefore be deduced from the experimental absorption spectrum. Our confidence in the self-consistency of above mentioned spectral decomposition comes from two observations: (a) S_R calculated from individual $S_{exp}(t)$ spectra fully resemble each other at all times (Fig. S20a, ESI†), thus validating the participation of only two species, and (b) increasing absorbance of the reorganized aggregate (A_{650}) correlates perfectly well with its calculated fraction ($1 - a_H$) (Fig. S20c, ESI†). A red-shifted absorption maximum of S_R along with an increased oscillator strength suggests that the reorganized aggregate has a J-type character.[16] § A considerably weaker, blue shifted (~551 nm) absorption feature indicates a small rotational offset between the stacked dye molecules, thus rendering the forbidden higher-energy transition of the J-aggregate partially allowed. Different supramolecular aggregation pathways are known to be critically dependent on parameters such as concentration (C) and temperature (T).[17] Once confined inside the micellar core, an elevated local concentration and reduced molecular degrees of freedom (rotational and translational) can effectively mimic a "high C, low T" situation, in which a kinetically stabilized H-aggregate is initially formed that gradually transforms into a more stable J-aggregate. Quite interestingly, the encapsulated 2R-cNDI aggregates also display very unique thermal characteristics. Temperature dependent absorption spectroscopy reveals their remarkable stability against thermal dissociation, up to 60 °C (Fig. S21, ESI†), a temperature at which aggregates of several strongly pi-stacking PBI undergo significant disassembly.[18] This apparent thermal insulation offered by micellar encapsulation is also seen in our kinetics experiments (Fig. S18c and d, ESI†) as the rates of encapsulation, aggregation and subsequent H- to J-reorganization (in the case of 2R-cNDI) steps remain unaffected by a change in temperature.

Fig. 3 presents the steady-state absorption spectra of R-cNDI and 2R-cNDI dyes co-encapsulated (see the ESI† for details) within PMMA-*b*-PPEGMA micelles. Interestingly, the spectra can

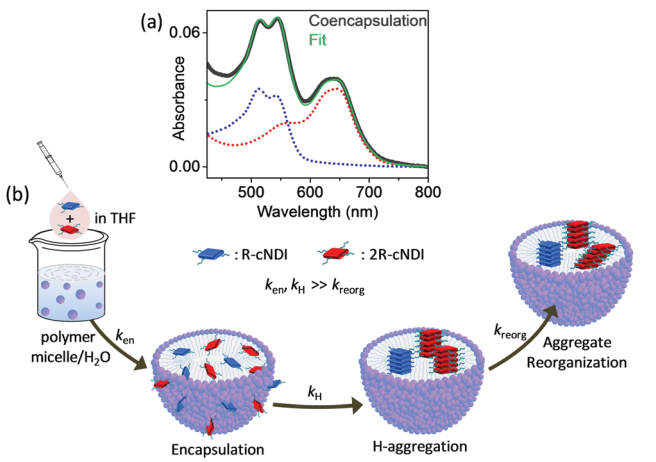

Fig. 3 Kinetic self-sorting. (a) Absorption spectra of R-cNDI and 2R-cNDI co-encapsulated within PMMA-*b*-PPEGMA micelles, expressed as a linear combination of the individual steady-state spectra of encapsulated R-cNDI (blue dot) and 2R-cNDI (red dot). (b) A schematic representation of encapsulation induced aggregation; k_{en}, k_H and k_{reorg} denote the rate constants of encapsulation, H-aggregation and subsequent aggregate reorganization steps.

be reliably expressed as a linear combination of the individual steady-state absorption spectra of encapsulated R-cNDI and 2R-cNDI, with the latter showing about 30% reduced uptake. This suggests that aggregation of the encapsulated dyes proceed fairly independently (Fig. 3b), resulting in a perfect self-sorting in the aggregate state.[19] We speculate that the observed self-sorting is an outcome of fast encapsulation followed by an equally fast H-aggregation kinetics discussed earlier, which precludes the formation of any mixed aggregate.

To conclude, we have demonstrated that spatial confinement offers a rapid and efficient strategy for molecular aggregation, particularly when intermolecular non-covalent interactions are too weak to accomplish the same. Local concentration and the entropy of the confined molecules are significantly different from those in solution, making it possible to realize unique geometries through different self-assembly pathways. The micellar core provides a significant degree of thermal stability/insulation to the encapsulated aggregates. Finally, fast aggregation kinetics allows a perfect self-sorting of aggregates.

The authors gratefully acknowledge IISER Kolkata and the Department of Science and Technology (DST), India (Project: EMR/2014/000223) for financial support. SS acknowledges UGC, and IM acknowledges CSIR for scholarship.

Notes and references

‡ London dispersion forces between the hydrocarbon side-chains are much shorter-range interactions ($1/r^6$) than pi-stacking ($1/r^5$) and are therefore, less likely to play a dominant role in the initial stages of self-assembly, when molecules are isolated and far from each other.
§ A coexistence of two kinds of aggregates within the tiny core of the micelle is likely to favour an efficient transfer of photoexcitation energy from the reorganized J- to H-aggregates, thus explaining a lack of PL from the former.

1 T. Aida, E. W. Meijer and S. Stupp, *Science*, 2012, **335**, 813; S. S. Babu, V. K. Praveen and A. Ajayaghosh, *Chem. Rev.*, 2014, **114**, 1973.
2 R. Klajn, J. F. Stoddart and B. Grzybowski, *Chem. Soc. Rev.*, 2010, **39**, 2203; D. Chaudhuri, D. Li, Y. Che, E. Shafran, J. M. Gerton, L. Zang and J. M. Lupton, *Nano Lett.*, 2011, **11**, 488; F. Würthner, C. R. Saha-Möller, B. Fimmel, S. Ogi, P. Leowanawat and D. Schmidt, *Chem. Rev.*, 2015, **116**, 962.
3 F. Würthner, *Acc. Chem. Res.*, 2016, **49**, 868; T. E. Kaiser, V. Stepanenko and F. Würthner, *J. Am. Chem. Soc.*, 2009, **131**, 6719.
4 Y. Wu, M. Frasconi, D. M. Gardner, P. R. McGonigal, S. T. Schneebeli, M. R. Wasielewski and J. F. Stoddart, *Angew. Chem., Int. Ed.*, 2014, **53**, 9476; J. Seibt, P. Marquetand, V. Engel, Z. Chen, V. Dehm and F. Würthner, *Chem. Phys.*, 2006, **328**, 354.
5 N. Sakai, J. Mareda, E. Vauthey and S. Matile, *Chem. Commun.*, 2010, **46**, 4225; V. Gorteau, G. Bollot, J. Mareda and S. Matile, *Org. Biomol. Chem.*, 2007, **5**, 3000.
6 F. Würthner, *Chem. Commun.*, 2004, 1564; F. Würthner, *Pure Appl. Chem.*, 2006, **78**, 2341.
7 T. Earmme, Y. J. Hwang, N. M. Murari, S. Subramaniyan and S. A. Jenekhe, *J. Am. Chem. Soc.*, 2013, **135**, 14960; X. Guo, F. S. Kim, M. J. Seger, S. A. Jenekhe and M. D. Watson, *Chem. Mater.*, 2012, **24**, 1434.
8 R. S. K. Kishore, O. Kel, N. Banerji, D. Emery, G. Bollot, J. Mareda, A. Gomez-Casado, P. Jonkheijm, J. Huskens, P. Maroni, M. Borkovec, E. Vauthey, N. Sakai and S. Matile, *J. Am. Chem. Soc.*, 2009, **131**, 11106.
9 S. V. Bhosale, C. Jani, C. H. Lalander and S. J. Langford, *Chem. Commun.*, 2010, **46**, 973; S. V. Bhosale, C. Jani, C. H. Lalander, S. J. Langford, I. Nerush, J. G. Shapter, D. Villamainac and E. Vauthey, *Chem. Commun.*, 2011, **47**, 8226; H. Kar, D. W. Gehrig, F. Laquai and S. Ghosh, *Nanoscale*, 2015, **7**, 6729; A. Das and S. Ghosh, *Chem. Commun.*, 2016, **52**, 6860; M. Al Kobaisi, S. V. Bhosale, K. Latham, A. M. Raynor and S. V. Bhosale, *Chem. Rev.*, 2016, **116**, 11685.
10 A. Datar, R. Oitker and L. Zang, *Chem. Commun.*, 2006, 1649.
11 N. C. Bell, S. J. Doyle, G. Battistelli, C. L. M. LeGuyader, M. P. Thompson, A. M. Poe, A. Rheingold, C. Moore, M. Montalti, S. Thayumanavan, M. J. Tauber and N. C. Gianneschi, *Langmuir*, 2015, **31**, 9707.
12 M. Sasikumar, Y. V. Suseela and T. Govindaraju, *Asian J. Org. Chem.*, 2013, **2**, 779.
13 K. Kataoka, G. S. Kwon, M. Yokoyama, T. Okano and Y. Sakurai, *J. Controlled Release*, 1993, **24**, 119.
14 Y. K. Che, X. M. Yang, K. Balakrishnan, J. M. Zuo and L. Zang, *Chem. Mater.*, 2009, **21**, 2930.
15 F. Würthner, Z. J. Chen, V. Dehm and V. Stepanenko, *Chem. Commun.*, 2006, 1188.
16 F. C. Spano, *Acc. Chem. Res.*, 2010, **43**, 429.
17 D. van der Zwaag, P. A. Pieters, P. A. Korevaar, A. J. Markvoort, A. J. H. Spiering, T. F. A. de Greef and E. W. Meijer, *J. Am. Chem. Soc.*, 2015, **137**, 12677; F. Fennel, S. Wolter, Z. Xie, P.-A. Plötz, O. Kühn, F. Würthner and S. Lochbrunner, *J. Am. Chem. Soc.*, 2013, **135**, 18722; E. Mattia and S. Otto, *Nat. Nanotechnol.*, 2015, **10**, 111.
18 S. Ogi, V. Stepanenko, K. Sugiyasu, M. Takeuchi and F. Würthner, *J. Am. Chem. Soc.*, 2015, **137**, 3300; C. Kulkarni, K. K. Bejagam, S. P. Senanayak, K. S. Narayan, S. Balasubramanian and S. J. George, *J. Am. Chem. Soc.*, 2015, **137**, 3924; F. Würthner, T. E. Kaiser and C. R. Saha-Möller, *Angew. Chem., Int. Ed.*, 2011, **50**, 3376.
19 M. M. Safont-Sempere, G. Fernández and F. Würthner, *Chem. Rev.*, 2011, **111**, 5784; A. Das, M. R. Molla and S. Ghosh, *J. Chem. Sci.*, 2011, **123**, 963.